

An $H\alpha$ survey of the rich cluster A 1689

Michael L. Balogh^{1,4}, Warrick J. Couch², Ian Smail¹, Richard G. Bower¹
& Karl Glazebrook³

¹*Department of Physics, University of Durham, South Road, Durham, DH1 3LE, UK*

²*School of Physics, University of New South Wales, Sydney 2052, Australia*

³*Department of Astrophysics, Johns Hopkins University, Baltimore, Maryland, USA*

⁴*email: M.L.Balogh@durham.ac.uk*

29 October 2018

ABSTRACT

We present results of an $H\alpha$ survey in the rich cluster A 1689 at $z = 0.18$, using the LDSS++ spectrograph on the AAT. We obtained spectra covering redshifted $H\alpha$ at $z = 0.16$ – 0.22 , for 522 galaxies brighter than $I = 22.5$, covering a field of $8.7' \times 8.7'$ ($\sim 1.1 \times 1.1 h^{-1}$ Mpc at $z = 0.18$). We securely detect $H\alpha$ emission in 46 of these galaxies; accounting for selection effects due to sampling and cluster membership, we determine that $24 \pm 4\%$ of cluster members brighter than $M_R = -16.5 + 5 \log h$ are detected with $H\alpha$ flux greater than $4h^{-2} \times 10^{38}$ ergs s^{-1} . This corresponds to a limiting star formation rate of $0.008 h^{-2} M_{\odot} \text{ yr}^{-1}$, assuming 1 magnitude of dust extinction. Our observations are sufficiently sensitive to detect galaxies with star formation rates comparable to that of the Milky Way ($\gtrsim 3 M_{\odot} \text{ yr}^{-1}$), unless they are obscured by more than 7 magnitudes of extinction. From a *Hubble Space Telescope* mosaic covering $7.5' \times 10.0'$, we determine morphologies for 199 galaxies brighter than $I = 21$, and find that $\sim 20\%$ of the cluster members are of type Sa or later. More than 90% of cluster spirals show $H\alpha$ emission, compared with less than 10% of E and S0 galaxies. The cluster $H\alpha$ luminosity function has a low normalisation relative to the $z \sim 0.2$ field, by $\sim 50\%$, after accounting for the different fraction of spiral galaxies in the two environments. When compared with local field galaxies, this suggests that star formation activity is suppressed in early-type cluster galaxies, relative to their field counterparts. Our sample includes 29 galaxies previously observed with *ISOCAM* at $6.7\mu\text{m}$ and $15\mu\text{m}$. We detect all $15\mu\text{m}$ sources at $H\alpha$, so there is no evidence for any star formation completely hidden at $H\alpha$. Comparing the $15\mu\text{m}$ and $H\alpha$ fluxes, we find evidence that some mid-infrared-detected galaxies could be obscured by as much as 3 magnitudes of extinction at $H\alpha$, although this depends on the largely unknown contribution from any AGN-heated dust to the mid-infrared flux.

Key words: galaxies:clusters

1 INTRODUCTION

There is an increasing body of observational evidence that star formation in the cores of galaxy clusters is much lower than that in the surrounding field, whatever the redshift (e.g., Balogh et al. 1997, 1998; Poggianti et al. 1999; Martin et al. 2000; Couch et al. 2001, hereafter Paper I). Although there is evidence that higher redshift clusters have a larger population of late-type, current or recently star-forming galaxies than local clusters (e.g., Butcher & Oemler 1984; Couch et al. 1998; Dressler et al. 1997; Margoniner et al. 2001; Kodama & Bower 2001), a similar increase in activity is also seen in the field (Lilly et al. 1995; Madau et al. 1996; Cowie et al. 1999). Thus, the increase in cluster

activity with redshift could simply reflect this, modulated by the changing rate of infall onto the clusters (Bower 1991; Ellingson et al. 2001).

However, most of the spectroscopic evidence for current or recent star formation in moderate to high redshift clusters comes from observations of the $[\text{OII}]\lambda 3727$ emission line. Unfortunately, $[\text{OII}]$ emission is sensitive to both metallicity effects and dust extinction (Kennicutt 1998; Jansen et al. 2000), and in both these respects the $H\alpha$ emission line provides a superior indicator of star formation. At moderate redshifts, however, $H\alpha$ is redshifted into a wavelength regime dominated by bright sky lines, and its observation requires

selecting a cluster for which $H\alpha$ lies in a window between these lines (Paper I; Balogh & Morris 2000).

There remains the intriguing possibility that a substantial amount of star formation (in clusters and elsewhere) is obscured by dust, thus rendering even $H\alpha$ surveys incomplete (Blain et al. 1999; Smail et al. 1999; Dwarakanath & Owen 1999; Poggianti & Wu 2000). Dust heated by star formation activity will radiate at mid-infrared (MIR) wavelengths, and thus such optically-obscured star formation may be recovered in MIR surveys. Evidence suggests that most of the MIR emission in local spiral galaxies is due to star formation (Genzel et al. 1998; Lutz et al. 1998; Fadda et al. 2002; Roussel et al. 2001), but this is still controversial because the spectral shape of any contribution to the MIR from AGN-heated dust is uncertain (Tran et al. 2001). If most of the MIR emission originates from starburst-heated dust, then observations suggest that much of the star formation in the universe is optically obscured by this dust (Rowan-Robinson et al. 1997; Flores et al. 1999; Roche & Eales 1999; Rigopoulou et al. 2000). Further complicating the issue is that the MIR population evolves strongly with redshift, which could indicate that the relative contributions of AGN- and starburst-heated dust are strongly redshift dependent (Almaini et al. 1999; Fabian & Iwasawa 1999; Alexander et al. 2001; Wilman et al. 2000). Such complications make the analysis and interpretation of current MIR surveys time-consuming.

Recently, Fadda et al. (2000) presented *ISOCAM* observations of the $z = 0.18$ cluster A 1689 at $6.7\mu\text{m}$ and $15\mu\text{m}$. At the cluster redshift, the $6.7\mu\text{m}$ filter covers the tail of stellar emission and aromatic carbon compounds associated with star formation, while the $15\mu\text{m}$ filter is dominated by the hot dust continuum. Fadda et al. (2000) showed that A 1689 contains an excess of $15\mu\text{m}$ sources relative to local clusters, suggesting that the cluster hosts a population of dusty starburst galaxies. We observed A 1689 in April 2001, with the upgraded Low Dispersion Survey Spectrograph (LDSS++; Glazebrook & Bland-Hawthorn 2001) on the 3.9m Anglo-Australian Telescope (AAT), as part of a larger program to measure $H\alpha$ in a diverse sample of four $z \sim 0.2-0.3$ clusters (see Paper I for initial results). Our observational technique allows deep, efficient measurements of $H\alpha$ to be made, and moreover gives precise dynamical information and allows us to identify the presence of AGN from the relative strength of the adjacent [NII] line. In this paper we present the results of these observations, comparing the population of emission line galaxies with the surrounding field and also our previously published $H\alpha$ survey of the $z = 0.31$ cluster AC114 (Paper I). These observations include 29 galaxies which were detected in the MIR by Fadda et al. (2000), which provides the opportunity to compare $H\alpha$ and MIR fluxes for a well defined, volume-limited sample.

The paper is organized as follows. Our spectroscopic observations with LDSS++, including the measurement of $H\alpha$ and the statistical correction for the sampling strategy, are described in §2.1. The *Hubble Space Telescope* (*HST*) observations are described in §2.2, and the data catalogue is presented in §2.3. In §3 we present the $H\alpha$ detections and their dependence on cluster radius, galaxy morphology, and MIR luminosity. The implications of the results are discussed in detail in §4, and summarized in the conclusions, §5. Throughout the paper we assume a cosmology

with $\Omega_\Lambda = 0.7$, $\Omega_m = 0.3$, and parameterise the Hubble parameter as $H_0 = 100h \text{ km s}^{-1} \text{ Mpc}^{-1}$.

2 OBSERVATIONS, REDUCTIONS AND ANALYSIS

2.1 LDSS++ Spectroscopy

2.1.1 Mask design and observations

The observations were made on the nights of 2001 April 23-24, using the LDSS++ on the AAT. We use the nod-and-shuffle technique described in Paper I, which allows for high-precision sky-subtraction in the presence of time-varying night-sky emission, and obviates the need for long slits (in order to get good sampling of the sky adjacent to the object); consequently, it is possible to work with very small apertures (circular micro-slits of $2''$ diameter) in the focal plane mask and thus observe many more objects simultaneously. The dispersion is $\sim 2.7 \text{ \AA}$ per pixel, with a spectral resolution $\sim 8 \text{ \AA}$ FWHM. As in Couch et al., we use a blocking filter to restrict our spectral coverage to the wavelength window in which the $H\alpha$ emission from cluster members would be seen, $\lambda = 7600\text{\AA}-8000\text{\AA}$. This enables us to overlap microslits in the wavelength direction, and hence to further increase the multiplex gain. The average cluster redshift is $z = 0.183$, with a velocity dispersion of $\sigma \sim 1989 \text{ km s}^{-1}$ (Struble & Rood 1999), although this latter value is likely inflated due to the presence of substructure along the line of sight (Girardi et al. 1997; Clowe & Schneider 2001). The $3-\sigma$ membership limits are then $z = 0.159-0.206$. $H\alpha$ will fall into our band limiting filter for $z = 0.158-0.224$; therefore we will detect $H\alpha$ in some background galaxies.

A single LDSS++ mask was created, with galaxy targets selected from a deep *I*-band image taken with the European Southern Observatory's New Technology Telescope (NTT) in $0''.9$ seeing conditions. We first allocated slits to 34 MIR sources (29 of which turned out to be galaxies), the maximum number possible with a single mask, comprising 75% of the sample published by Fadda et al. (2000). The remaining slits were assigned randomly to galaxies brighter than $I = 22.5$, with higher priority given to brighter galaxies. In total, we allocate 559 microslits over the full $8.7' \times 8.7'$ ($1.1 \times 1.1 h^{-1} \text{ Mpc}$ at $z = 0.18$) field-of-view of LDSS++.

The observations were obtained in reasonable weather conditions, with a total exposure time of 19.5 ks, of which half was on the objects and half on sky. To overcome the 50% losses due to having to obtain sky observations through the mask, we also experimented with placing mask holes in the position of the galaxy in the nominal "sky" position ($5''$ north of the target). However, none of these 76 positions yielded useful additional data, possibly due to guiding problems when off-target, so we have removed them from the present analysis. To ensure that our survey sampled even the most compact cluster members (e.g., Drinkwater et al. 1999), we were deliberately conservative in our star-galaxy separation, and subsequent comparison with *HST* imaging revealed 37 of our targets to be stars. Thus, our final sample consists of spectra for 522 galaxies.

The data reduction for nod-and-shuffle observations is very simple, requiring only that the spectra obtained from the two nodded positions be subtracted from one another. In

Paper I we noted that differences in scattered light across the detector meant the continuum level in the sky-subtracted object was uncertain, and had to be corrected for. For the data in the present paper, we subtracted a surface fit to the background light on the detector, rejecting light from the slits themselves. This removes the scattered light problem, and no further correction was necessary. Wavelength calibration is based on four lines from a CuAr arc lamp.

2.1.2 Flux Calibration

The conversion from detector counts to flux was achieved using the procedure described in Paper I. Nine galaxies with colours typical of early-type cluster members were identified, five of which are confirmed morphologically to be early-types. The galaxies are relatively isolated, and cover the magnitude range $I = 16.4\text{--}18.4$. The I -band flux within a $2''$ diameter aperture, corresponding to our microslit size, is computed from the NTT image, convolved to match the $\sim 2''$ seeing of the spectroscopic observations. This is converted to flux units at $\lambda = 7700\text{\AA}$, assuming a spectral shape $f_\nu \propto \nu^{-2.2}$, which is consistent with the observed $V - I \approx 1.6$ colours of these galaxies. This flux is compared with the average counts per \AA in the spectrum, over $\lambda = 7700\text{\AA}\text{--}8000\text{\AA}$. The calibration factor is $(2.0 \pm 0.4) \times 10^{-19} \text{ ergs s}^{-1} \text{ cm}^{-2} \text{ counts}^{-1}$, where the uncertainty represents the scatter between the nine galaxies. Note that this calibration indicates a factor ~ 4.3 increase in sensitivity relative to our AC114 observations (Paper I), reflecting the superior seeing conditions and transparency during which the A 1689 data were obtained. Measurements are not corrected for aperture effects or dust extinction. We note that there is no apparent correlation of flux calibration with position on the detector, over and above the uncertainties of the calibration itself.

Star formation rates are calculated from $H\alpha$ luminosities $L_{H\alpha}$, using the relation $\text{SFR}(M_\odot \text{yr}^{-1}) = 2.0 \times 10^{-41} L_{H\alpha} (\text{ergs s}^{-1})$ including 1 magnitude of dust extinction (Kennicutt 1998). Note that, throughout this paper, $H\alpha$ fluxes are presented as measured, while this average, estimated dust correction is applied to the star formation rates.

2.1.3 $H\alpha$ Detection and measurement

As in Paper I, the detection of $H\alpha$ emission lines in our spectra was done manually. Each spectrum was examined in its 2-D and optimally extracted 1-D form, while blinking with the corresponding sky spectrum. At the cluster redshift $z = 0.181$, $H\alpha$ lies in the middle of a forest of OH emission lines in the night sky spectrum. However, the nod-and-shuffle technique greatly reduces the number of night sky line residuals that remain over and above expected Poisson noise, after sky subtraction. In addition, the 2-D images are very useful for distinguishing real emission lines from noise fluctuations near bright sky lines, as the flux from real features is spread over more pixels.

Each spectrum was first examined and classified independently by MLB and WJC. The two lists were then compared, and discrepancies were re-examined. The majority of discrepancies were quickly resolved. Case I galaxies are

those with a clear $H\alpha$ detection, and at least one other emission line to confirm that the identification is correct. Usually these supporting lines were one of the $[\text{NII}]\lambda\lambda 6548, 6583$ lines; sometimes the $[\text{SII}]\lambda\lambda 6717, 6731$ lines were also visible. Emission lines with no supporting lines, or which could not be confidently distinguished from sky residuals, are defined as Case II, and are less secure detections. Where possible, we compared our detections with the redshifts subsequently published by Duc et al. (2002). This revealed only one $H\alpha$ identification (a Case II object) to be incorrect, as it was in fact an $[\text{OIII}]\lambda 5007$ emission line. Our remaining detections are consistent with the Duc et al. (2002) redshifts where available; in cases where the Duc *et al.* redshift confirms a Case II detection, we upgrade the quality to Case I.

We then measure the strength of the $H\alpha$ and adjacent $[\text{NII}]$ lines by fitting a line to the continuum blueward and redward of the three lines, and summing the flux above the continuum over the relevant line bandpass. Specifically, for $H\alpha$, we compare the flux at $\lambda = 6555\text{\AA}\text{--}6575\text{\AA}$ with the fit to the continuum at $\lambda = 6510\text{\AA}\text{--}6540\text{\AA}$ and $\lambda = 6590\text{\AA}\text{--}6620\text{\AA}$. For $[\text{NII}]\lambda 6583$, we define the feature at $\lambda = 6577\text{\AA}\text{--}6589\text{\AA}$, with the same continuum regions as $H\alpha$. The error vector is computed from the sky and object spectra, taking into account the gain (0.37 e^- per ADU) and read noise (1.8 e^- per pixel) of the detector. We use this error vector to calculate accurate uncertainties on the measured line fluxes. No correction is made for stellar absorption. Typically, the contribution from absorption is expected to be $\sim < 5\text{\AA}$ (Kennicutt 1992; Charlot et al. 2002), although the true correction depends on the past star formation history. The $H\alpha$ fluxes are only significantly ($> 20\%$) underestimated when the measured equivalent width is comparable to the absorption correction.

The spectra are sky-noise dominated; thus the *r.m.s.* in a feature-free region of the continuum gives a reasonable estimate of the noise level, independent of galaxy flux. Indeed, we find the *r.m.s.* of a random sample of galaxies to be approximately constant, at ~ 40 counts per pixel, although there is some dependence on wavelength, due to the presence of bright emission lines in the sky spectrum. A typical $H\alpha$ emission line has a FWHM of ~ 6 pixels; a 3σ detection therefore corresponds to $3 \times 40/\sqrt{6} \sim 50$ counts above the continuum. From the flux calibration computed in §2.1.2, our detection limit is thus approximately $1 \times 10^{-17} \text{ ergs s}^{-1} \text{ cm}^{-2}$, or $4h^{-2} \times 10^{38} \text{ ergs s}^{-1}$ at $z = 0.18$. From Kennicutt (1998), including 1 magnitude of extinction, this flux corresponds to a star formation rate of $0.008 h^{-2} M_\odot \text{ yr}^{-1}$. We therefore expect that $H\alpha$ emission from galaxies with star formation rates comparable to that of the Milky Way ($\sim 3 M_\odot \text{ yr}^{-1}$), will be detected unless they are obscured by more than seven magnitudes of extinction at $H\alpha$. This work represents the deepest $H\alpha$ observations at $z \gg 0$ to date; locally the only observations which are comparable in depth are the very recent data on Coma and Abell 1367, by Iglesias-Páramo et al. (2002).

2.1.4 Statistical Weights

To reliably compute global properties of the cluster our galaxy sample needs to be weighted by two factors. The first, which we call the sampling rate, accounts for the fact that only a fraction of the galaxies in the I -selected sample

were observed spectroscopically. In addition, some fraction of the galaxies observed, but for which $H\alpha$ was not detected, will not be cluster members, but rather belong to the foreground or background field. This “membership” correction is only applicable to galaxies which are not detected in $H\alpha$, since their redshifts are unknown. Both of these weights depend on galaxy I -magnitude and projected radius from the cluster centre.

The sampling rate as a function of I magnitude is shown in Figure 1a. All galaxies need to be weighted by the inverse of this fraction, to account for the frequency of such galaxies in a complete, magnitude limited spectroscopic survey. To determine the membership correction, we compare the number counts in our I -band image with the field number counts of Metcalfe et al. (2001). The expected fraction of cluster members determined in this way is also shown in Figure 1a. Some of that expected fraction are actually detected in $H\alpha$; thus, to determine the fraction of $H\alpha$ -undetected galaxies which are expected to be cluster members we need to subtract the fraction of detected galaxies from the expected fraction of cluster members. We present this in Figure 1b, where the fraction of $H\alpha$ -detected galaxies is shown as a function of I -band magnitude. The solid points show the difference between the cluster membership fraction and the detected fraction; this gives the fraction of galaxies undetected in $H\alpha$ that are expected to be members.

The combination of these two luminosity-dependent weights (depending on whether or not $H\alpha$ is detected) is called w_{lum} . A similar weight, w_{rad} , is computed to correct for the variation in sampling and membership with radius, as shown in Figure 1c. We renormalise w_{rad} so that the sum of the total galaxy weights, $w_{lum} \times w_{rad}$, is equal to the sum of w_{lum} .

There is potentially another selection bias, as radial annuli are incomplete at radii beyond ~ 175 arcsec, due to the rectangular geometry of the detector. Thus, galaxies at large radii are underrepresented in the photometric catalogue. In the absence of a strong radial gradient, however (see §3.2), this does not have a significant effect on our results.

2.2 Hubble Space Telescope Data

The *HST* WFPC2 imaging of A 1689 was obtained from the ST-ECF archive. These data come from the Cycle 5 programme, GO 5993, and comprise a total of 30 orbits exposure on 15 pointings spread across a $7.5' \times 10.0'$ field centred on the cluster core. Each of the 15 pointings was observed in two exposures totalling 2.3 ks in the F814W (I_{814}) passband and a further two exposures totalling 1.8 ks through the F606W (V_{606}) filter. These four exposures were each spatially offset by integer pixel shifts. Unfortunately, with only two exposures in a given passband it is difficult to reliably reject cosmic ray events and hot pixels when processing the images. For this reason we chose the unusual step of combining both passbands into a single composite F606W+F814W image. This combination benefits from the close similarity of galaxies between the two passbands; for galaxies at the redshift of the cluster the range in colours is only $V_{606} - I_{814} = 0.7\text{--}1.1$ for SEDs spanning Scd to E/S0. Thus by suitably scaling the two passbands we can combine them to produce cosmetically clean images for the bulk of the galaxies used in our analysis. These data have been pre-

viously used in the analysis of *ISOCAM* sources in the field of A 1689 by Duc et al. (2002).

We subsequently calibrate this image onto the I -band using our ground-based imaging, which also provides absolute astrometric calibration. The final mosaic covers a field of 69 sq. arcmin with $0.17''$ resolution, a per-pixel exposure time of 4.1 ks and an effective point-source sensitivity limit of $I \sim 26$.

The morphologies of the brighter galaxies in the *HST* field ($I < 21$) have been visually classified by one of us (WJC) onto the revised Hubble scheme used by the MORPHS project (see Smail et al. 1997). The presence of close neighbours, or signs of interactions such as tidal tails, were also noted.

2.3 The Catalogue

Our data and derived quantities are available electronically from *MNRAS*; a sample is shown in Table 1. Galaxies are identified by a unique number (column 1) and their J2000 coordinates (columns 2-3). The identification numbers below 50 correspond to the identification numbers in the MIR catalogue of Fadda et al. (2000). The I -band magnitude is given in column 4 and, where $H\alpha$ is detected, we show the quality classification (I or II), redshift and flux in columns 5-7. The corresponding [NII] flux is given in column 8, and derived star formation rates are in column 9. Morphological classifications, based on the *HST* images, are listed in column 10.

3 RESULTS

3.1 $H\alpha$ -Detected Galaxies

$H\alpha$ emission was detected in 60 of the 522 galaxies observed. Forty-six of these are Case I detections, 42 of which lie within $z = 0.159\text{--}0.206$ and are therefore associated with the cluster. Correcting for sampling frequency and cluster membership (§2.1.4), the fraction of Case I detections is $24 \pm 4\%$. This is comparable to the high fraction of blue galaxies brighter than $R = 22.7$ (at least 15%, possibly as high as 25%) found by Duc et al. (2002).

The $H\alpha$ luminosity function ($H\alpha$ LF) is shown in Figure 2, for both Case I and II detections. We impose a magnitude limit of $I < 22.5$ and adopt a cluster membership criteria of $z = 0.159\text{--}0.206$. Applying the sampling and membership corrections as discussed in §2.1.4, to the 504 galaxies observed with $I < 22.5$, we expect 328 cluster members in a complete sample to this depth. Considering only the Case I detections, the best fit Schechter (1976) parameters of this distribution are $\alpha \sim -0.1$, $L^* \sim 10^{40.0}$ ergs s^{-1} , steeper and with a fainter L^* than the recently measured local cluster $H\alpha$ LF ($\alpha \sim -0.7$, $L^* \sim 10^{40.6}$ ergs s^{-1} , Iglesias-Páramo et al. 2002).

We now compare the cluster $H\alpha$ LF with that of the field at $z \sim 0.2$, from the CFRS (Tresse & Maddox 1998, hereafter TM98). To compute the normalisation, we first note that the luminosity range covered by the CFRS is similar to ours. The CFRS samples galaxies with $-23.5 < M_{B_{AB}} < -15.5$ mag ($h = 1$); using the typical colour of a Sbc galaxy at $z = 0.2$ (Fukugita et al. 1995), this corresponds to

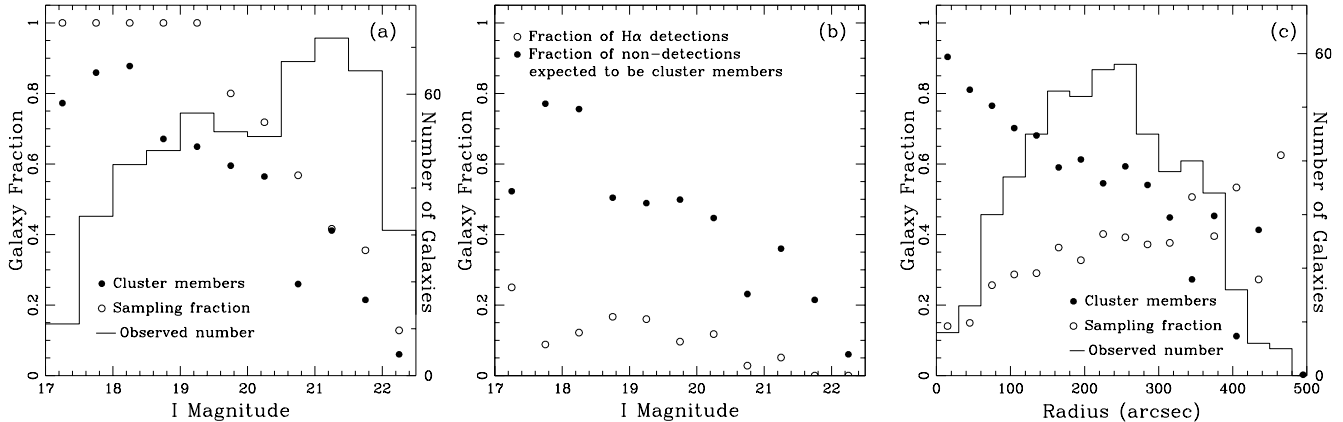


Figure 1. The determination of luminosity-dependent selection weights applied to the data. (a) The *open symbols* are the fraction of galaxies in our *I*-band NTT image for which we obtained a spectrum. All galaxies need to be weighted by the inverse of this number to estimate the corresponding number in the full photometric catalogue. *Solid symbols* are the fraction of galaxies expected to be cluster members as a function of *I* magnitude, computed as the difference between our number counts and the field counts of Metcalfe et al. (2001). The total number of galaxies in the sample is shown as the histogram, with scale on the right axis. (b) *Open symbols* are the fraction of Case I $H\alpha$ detections, as a function of *I*-band magnitude. The *solid points* show the difference between the expected fraction of cluster members and the fraction of $H\alpha$ detections. Only galaxies which are not detected in $H\alpha$ need to be weighted by this number, to account for field contamination. (c) As panel (a), but for the radial-dependent selection function.

Table 1.

SAMPLE A 1689 DATA

(1) Id	(2) R.A. (J2000)	(3) Dec	(4) I (mag)	(5) $H\alpha$ Class	(6) Redshift	(7) $H\alpha$ flux (10^{-17} ergs s $^{-1}$ cm $^{-2}$)	(8) [NII] λ 6583 flux (10^{-17} ergs s $^{-1}$ cm $^{-2}$)	(9) SFR ($h^{-2} M_{\odot}$ yr $^{-1}$)	(10) Morphology
3	13 11 25.354	-1 20 37.06	17.90	I	0.192	17.5 ± 6.2	17.0 ± 5.3	0.203 ± 0.072	Sab
4	13 11 27.109	-1 20 58.42	18.89	I	0.214	19.4 ± 6.3	5.1 ± 5.1	0.288 ± 0.094	Scd
6	13 11 27.681	-1 21 07.19	19.34	I	0.215	13.9 ± 6.2	-0.9 ± 4.9	0.208 ± 0.093	Sd
7	13 11 27.821	-1 20 07.76	17.69	-	-	-	-	-	E
...									

$-25.6 < M_I < -17.6$. The faint end of this limit corresponds to $I = 22.5$, which is where we limit our sample. Over this luminosity range, TM98 find $110/131=84\%$ of galaxies have $H\alpha$ flux greater than $3 \times 10^{39} h^{-2}$ ergs s $^{-1}$. Thus, we normalise the CFRS $H\alpha$ LF so that 275 galaxies (84% of 328) have luminosities greater than this limit. TM98 correct their observed fluxes for reddening on a galaxy-by-galaxy basis, while we choose to present our data uncorrected for reddening; thus, for comparison we reduce the CFRS $H\alpha$ fluxes by a factor of 2.0, corresponding to their average measured $H\alpha$ extinction. Finally, TM98 also estimate a correction for flux missed by their $1''.75$ aperture, which increases their fluxes by a factor which is 1.6 in the mean, but which can be as large as a factor of 4. As we do not correct for aperture effects, we reduce the CFRS $H\alpha$ fluxes by a uniform factor of 1.6, to make a more fair comparison with our $2''$ apertures. Note that these corrections were not made in Paper I. The normalisation of the cluster $H\alpha$ LF is low, relative to that of the field, by a factor of ~ 5 . Thus the total amount of ongoing star formation in this cluster is much less than in the field, as found in most, if not all, high-density environments (e.g., Balogh et al. 1997; Poggianti et al. 1999; Martin et al. 2000, Paper1).

We also show a direct comparison with our previous

work on AC114 (Paper I) in Figure 2. Our AC114 observations are statistically complete (after application of a luminosity-dependent weight to account for membership and selection fractions) to $I = 22.25$ ($M_R \sim -16.5 + 5 \log h$). In the cosmology we use, this luminosity limit in A 1689 corresponds to $I = 20.9$, so the latter samples galaxies 1.6 mag less luminous than AC114. The AC114 $H\alpha$ LF is normalized to a total of 244 cluster members, the weighted number of members in A 1689 brighter than $I = 20.9$. Only Case I detections are considered.

The number of galaxies detected in $H\alpha$ is about two times larger in A 1689, than in AC114. The reason for this difference is not completely understood; both clusters have a large fraction of blue galaxies (10-20%, Couch & Sharples 1987; Duc et al. 2002), and any effects of global evolution would lead to more star formation in the higher redshift cluster AC114, contrary to what is observed. The most likely reason for the difference is in the dynamical state of the clusters. AC114 is highly elongated across the sky, but appears to be fairly relaxed. On the other hand, although A 1689 has a smooth, spherical X-ray morphology (Durret et al. 1994), there is clear evidence of substructure in the galaxy distribution along the line of sight (Girardi et al. 1997; Duc et al. 2002), and it appears to be a dynamically active (i.e.

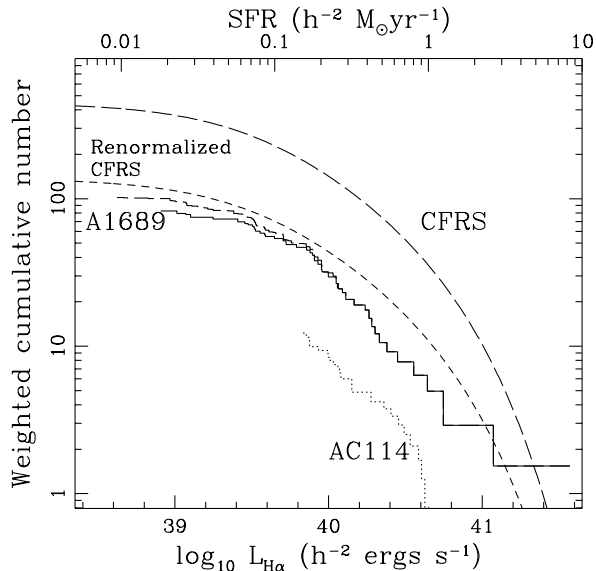


Figure 2. The $H\alpha$ luminosity function of A 1689, compared with that of the CFRS (TM98). Both the Case I (*solid line*) and II (*long dashed line*) functions are shown. The CFRS luminosity function is uncorrected for aperture effects and reddening, to allow a fair comparison with our data. We also show this luminosity function renormalized to account for the different morphological composition of the cluster and field samples, as described in §4 (*short-dashed line*). Finally, we show the luminosity function of AC114, from Paper I, renormalized to the number of cluster members in A 1689 brighter than $I = 20.9$, corresponding to the equivalent luminosity limit in AC114.

merging) cluster. We will explore this difference in detail in later work, when we compare the $H\alpha$ properties of all four morphologically diverse clusters in our program.

3.2 The Galaxy Distribution

The dynamical properties of the $H\alpha$ population are shown in Figure 3, where we compare the redshift distribution of the Class I $H\alpha$ detections with that of the magnitude limited, V -selected spectroscopic survey of Duc et al. (2002). First, we point out that the velocity distribution of the cluster is highly non-Gaussian, with evidence for substructure in the foreground and background, as previously noted (Girardi et al. 1997). Thus, the virialized cluster is probably less massive than naively expected from the very high velocity dispersion of $\sigma \sim 1989 \text{ km s}^{-1}$ (Struble & Rood 1999); from weak lensing measurements, Clowe & Schneider (2001) find that the central structure is well fit as an isothermal sphere with $\sigma = 1028 \text{ km s}^{-1}$. Most interestingly, the $H\alpha$ detections do not show a peak at the mean cluster redshift of $z = 0.183$, but rather appear to be associated with the substructure at $\sim 1600 \text{ km s}^{-1}$ in front of and behind the cluster. They could either be associated with a galaxy population which is infalling at high velocity, or with approximately virialized subgroups $\sim 20 \text{ Mpc}$ in front of and behind the main cluster. Either way, these galaxies are not virialized in the main cluster potential, but are likely to be in the process of being accreted. This provides good support for models in which cluster gradients in star formation activity is related to the

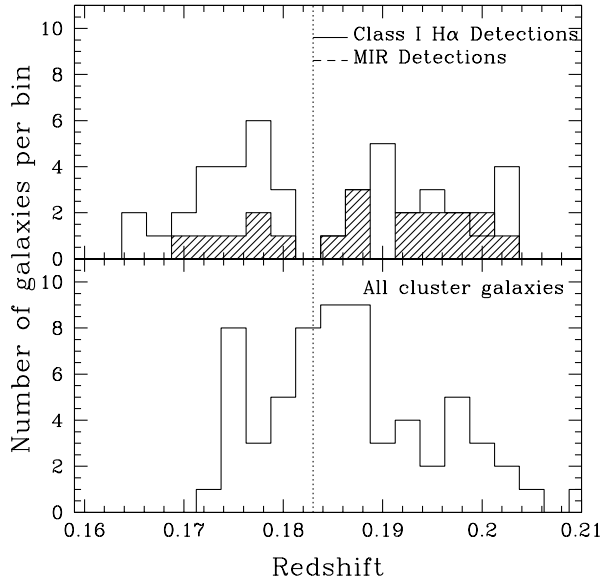


Figure 3. Top: The *open histogram* is the redshift distribution of the Class I $H\alpha$ detections, while the *shaded histogram* is the distribution of the MIR detections from Fadda et al. (2000). **Bottom:** The redshift distribution of the galaxies from the redshift sample of (Duc et al. 2002). The vertical *dotted line* is the mean cluster redshift from Struble & Rood (1999), $z = 0.183$.

infall of galaxies (e.g., Balogh et al. 2000; Ellingson et al. 2001). We also show in Figure 3 the redshift distribution of the galaxies detected in the MIR (Fadda et al. 2000). These galaxies show a similar distribution to the $H\alpha$ sample, suggesting that they are tracing the same population.

The spatial distribution of the targetted galaxies brighter than $I = 22.5$ is shown in Figure 4. The $H\alpha$ detections in the low- and high-redshift substructures do not appear to correspond to spatially distinct structures in projected position. If they do correspond to foreground/background structures, then, both of these are spread across our full field of view.

In Figure 5 we show the weighted fraction of Class I $H\alpha$ detections as a function of distance from the central galaxy (#20), in Mpc. There is no evidence for a trend in the fraction of $H\alpha$ emitters with radius out to $\sim 1h^{-1} \text{ Mpc}$. At all radii the fraction is less than $\sim 50\%$, well below that of the field at this redshift, $\sim 85\%$ (TM98). A 1689 is a very massive cluster, with an estimated virial radius of $r_v \sim 2.8 \text{ Mpc}$, based on a velocity dispersion of 1028 km s^{-1} (Clowe & Schneider 2001) and the virial r_v - σ relation of Girardi et al. (1998). Thus, these observations are only probing the core, within $0.4r_v$, which may explain the lack of a strong gradient in emission line galaxy fraction, relative to other studies (e.g., Balogh et al. 1997). Furthermore, we reiterate that the emission appears to be entirely restricted to the structures in the foreground and background of the main cluster, which serves to dilute any radial gradient present.

3.3 Galaxy Morphologies

HST imaging is available for 199 of the galaxies in our survey brighter than $I = 21$. For purposes of presentation we

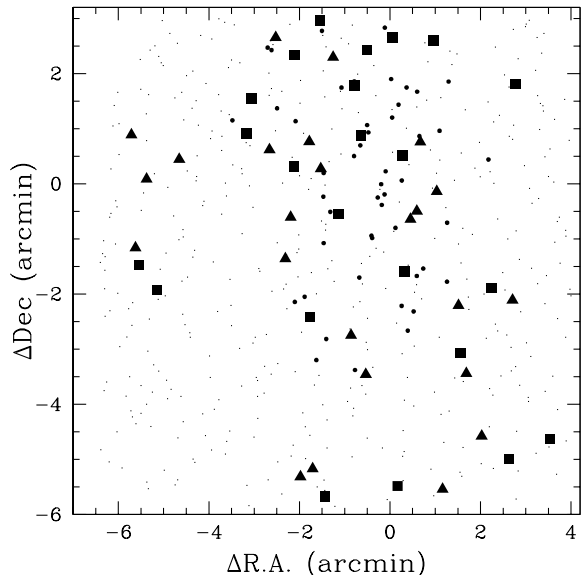


Figure 4. The spatial distribution of the targetted galaxies in A 1689, brighter than $I = 22.5$. The *small dots* indicate the position relative to the central galaxy for each galaxy for which a spectrum was obtained. The *filled circles* are those galaxies which are known to be cluster members, from the spectroscopy of Duc et al. (2002). The *large, filled symbols* are those galaxies we detect at $H\alpha$; the *filled squares* are those with $z < 0.185$, while the *filled triangles* are those with $z > 0.185$.

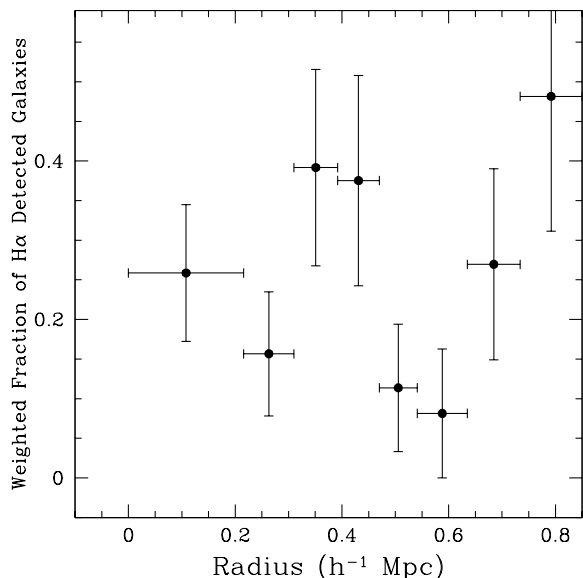


Figure 5. The fraction of Case I $H\alpha$ detections as a function of distance from the central cluster galaxy, for galaxies brighter than $I = 22.5$. The fractions are weighted to account for the varying sampling frequency and cluster membership as a function of magnitude and radius, as described in the text. Radial bins are of varying width, so that each bin includes an equal number (~ 60) of galaxies. The error bars in the vertical direction are computed assuming Poisson statistics, and those in the horizontal direction represent the size of the radial bin.

have divided the galaxies into five classes: Elliptical (E), S0 (including E/S0 and S0/a), Sab (including Sa, Sb, Sab), Scd (including Sc, Sd, Scd and Irr) and Uncertain (usually because the galaxy lies at the edge of the *HST* field).

To determine the morphological distribution of the cluster population, it is necessary to correct for contamination from the foreground and background field. We will consider two ways of doing this. The first is to use the redshifts obtained by Duc et al. (2002), and to only consider galaxies within the redshift range $z = 0.159$ – 0.206 . This limits our sample to 60 galaxies. The distribution of morphological types among confirmed cluster members is shown in the top panel of Figure 6a. The cluster is dominated by early-type galaxies; only $20 \pm 6\%$ of galaxies are of Hubble type Sa or later. In the bottom panel we show the fraction of each galaxy type that is detected in $H\alpha$. The detections are almost entirely restricted to spiral galaxies; only 3/46 (6.5%) of the early-type galaxies are securely detected in $H\alpha$.

Although the detection rate of spiral galaxies appears to be high, the uncertainties are large because of the small number (12) of late type galaxies in the sample. In particular, there are only 2 Scd-type galaxies, so the 100% detection rate is very uncertain. Another approach is to make a statistical correction similar to that used in §2.1.4, assuming a field morphological composition of 15% E, 20% E/S0, 30% Sab and 35% Scd as determined from the Medium Deep Survey morphological classifications to an equivalent magnitude limit to that considered here (Abraham et al. 1996; Glazebrook et al. 1995). We describe this procedure more thoroughly in the Appendix. In Figure 6b we show the analogue of Figure 6a, but now using the larger sample and statistically correcting for the field contribution. The conclusions are similar, and it is encouraging that the fraction of cluster spiral galaxies is $22 \pm 4\%$, in excellent agreement with the fraction determined from the subsample with redshifts. The detection rate for $H\alpha$ emission from Sab and Scd galaxies is very high, greater than 90%. The fraction of early type galaxies securely detected in $H\alpha$ remains below 10%. We therefore find no difference between the fraction of late-type cluster galaxies detected in $H\alpha$ and the high fractions seen in local field samples (Kennicutt 1992; Jansen et al. 2000), a result we discuss in more detail in §4.

3.4 Mid-Infrared Sources

Of the 522 galaxies targeted, 29 were known MIR sources, from the *ISOCAM* observations of Fadda et al. (2000). Nineteen of these have measured redshifts $z = 0.158$ – 0.224 , so any $H\alpha$ emission will lie within our observable wavelength range (although we note that galaxies at $z > 0.206$ are behind the cluster as we have defined it). Another two MIR sources, which did not have known redshifts, were detected in $H\alpha$, bringing the total number of MIR sources which lie in the observable redshift range to 21.

MIR fluxes from Fadda et al. (2000) are available at $6.7\mu\text{m}$ and $15\mu\text{m}$ wavelengths, termed LW2 and LW3. Emission in the redder band comes predominantly from hot dust while the $6.7\mu\text{m}$ fluxes are dominated by stellar emission and aromatic carbon compounds related to star formation in late-type galaxies. Normal spiral galaxies at $z \sim 0.2$ are expected to have typical flux ratios of $L_{15\mu\text{m}}/L_{6.7\mu\text{m}} < 3.2$, while starburst galaxies should have relatively stronger

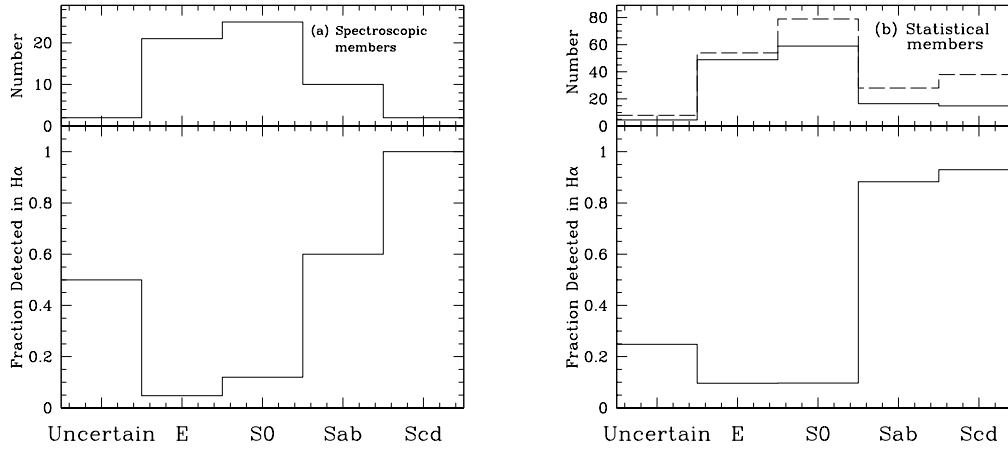


Figure 6. (a) **Top panel:** The number of galaxies brighter than $I = 21$ as a function of Hubble type is shown for confirmed cluster members, from the spectroscopy of Duc et al. (2002). **Bottom panel:** The fraction of spectroscopically confirmed cluster galaxies of each type securely detected in $H\alpha$. (b) Similar to (a) but for the full LDSS++ and *HST* sample, with a statistical field correction as described in the Appendix. Shown in the top panel is the observed morphological distribution (*dashed line*) and the distribution after making the statistical background subtraction (*solid line*).

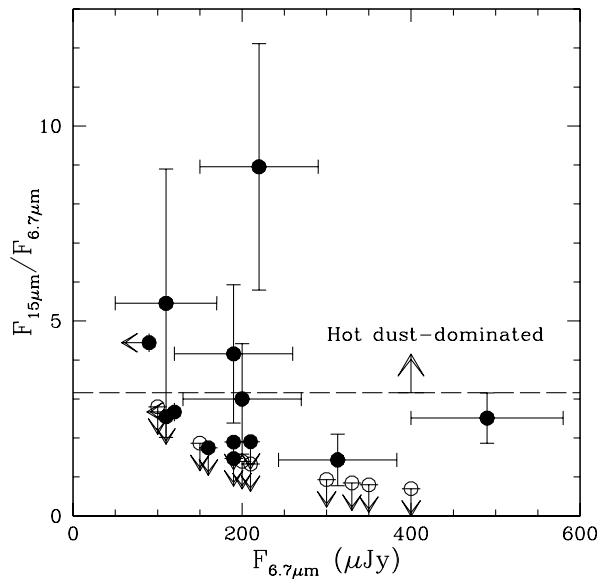


Figure 7. The ratio of the MIR flux at $15\mu\text{m}$ to the flux at $6.7\mu\text{m}$, as a function of $6.7\mu\text{m}$ flux for the 21 *ISO* sources from Fadda et al. (2000), included in the present study. The *filled symbols* represent those galaxies we have detected in $H\alpha$ emission, while the remainder are shown as *open circles*. The horizontal, *dashed line* shows an approximate division between normal spirals (below the line) and galaxies dominated by a hot-dust component (Laurent et al. 2000).

$15\mu\text{m}$ luminosities (Duc et al. 2002; Laurent et al. 2000). Spectra of dust-enshrouded AGN are also expected to be dominated by a hot dust component, with aromatic carbon bands similar to those seen in HII regions (Tran et al. 2001). Although the dust temperature and grain size distribution are expected to be different depending on whether the heating mechanism is star formation or an AGN, it is

not possible to distinguish the two mechanisms based only on the $L_{15\mu\text{m}}/L_{6.7\mu\text{m}}$ ratio (Laurent et al. 2000).

The MIR properties of the 21 *ISO* sources observed with LDSS++ are shown in Figure 7. All but two of these sources are detected at $6.7\mu\text{m}$, while only eight are detected at $15\mu\text{m}$. Half of the galaxies detected at $15\mu\text{m}$ are unusually bright at $15\mu\text{m}$, relative to that expected for normal spiral galaxies. These spectra are likely dominated by a hot dust component, although it is not clear from these data alone whether the dust is heated by star formation or by nuclear activity. In Figure 8 we show the continuum-subtracted LDSS++ spectra of the eight $15\mu\text{m}$ sources, and the 13 remaining galaxies detected only at $6.7\mu\text{m}$. Morphological and spectral classifications are labelled next to each spectrum. The spectral classifications are from Duc et al. (2002), while the morphologies are our own classifications.

Of the 13 MIR galaxies which are only detected at $6.7\mu\text{m}$, only 5 (38.5%) show $H\alpha$ emission. The remainder are early-type galaxies (E or S0), two of which clearly show $H\alpha$ in absorption. Thus it seems likely that the $6.7\mu\text{m}$ light is dominated by stellar emission, and does not directly trace the hot dust component. In stark contrast with this, *all* eight of the $15\mu\text{m}$ -detected sources are spiral galaxies securely detected in $H\alpha$. Thus, our deep $H\alpha$ survey recovers all the potentially-detected star forming galaxies found by *ISOCAM*.

From Figure 8b, it is evident that many of the $15\mu\text{m}$ galaxies have atypical spectra in the region of $H\alpha$. ISO#41 has very broad $H\alpha$ emission and was previously identified as a Seyfert 1 galaxy (Duc et al. 2002). Object #31 has a particularly unusual $H\alpha$ line profile. $H\alpha$ emission is detected at 7729\AA , corresponding to a redshift $z = 0.1777$; however, the redshift given by Duc et al. (2002), 0.1757, places $H\alpha$ at the absorption trough at 7716\AA . Therefore, it appears that the nebular emission is offset from the stellar absorption by $\sim 500 \text{ km s}^{-1}$. Three other galaxies, ISO#3, 10 and 37, show unusually strong $[\text{NII}]\lambda 6583$ emission; in Figure 9 we show the ratio of $[\text{NII}]\lambda 6583$ to $H\alpha$, as a function

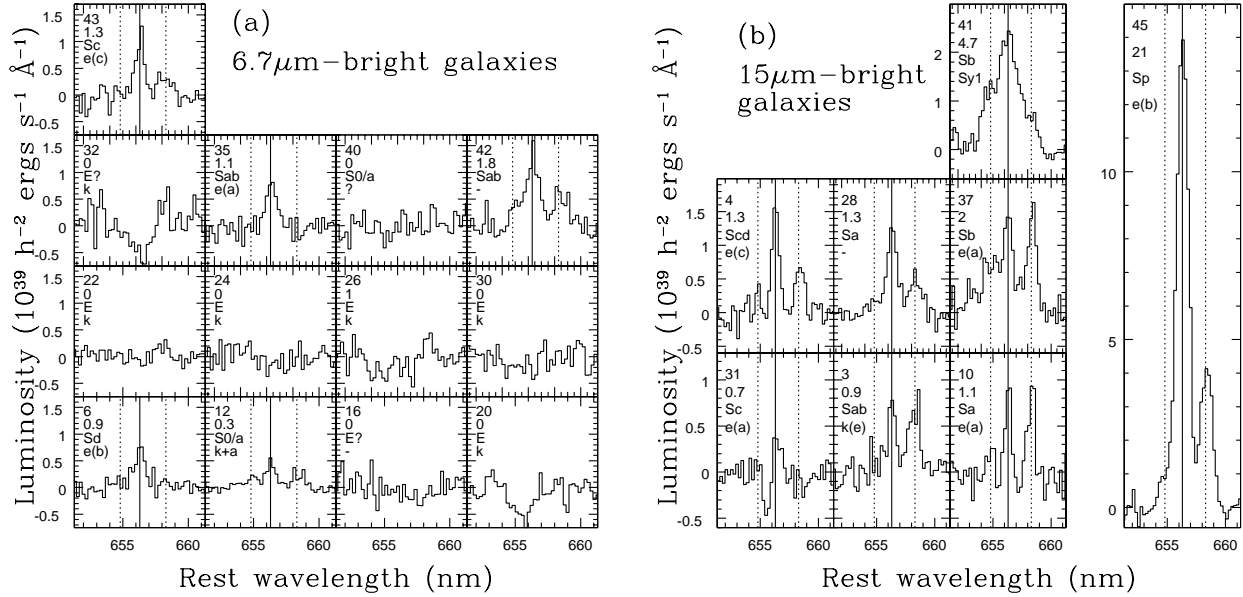


Figure 8. Continuum-subtracted, rest frame LDSS++ spectra of galaxies detected with *ISOCAM*. The top row in each box shows the ISO id number of the galaxy. The next number is the total H α flux in units of $10^{40} \text{ ergs s}^{-1}$, followed by the morphological classification and the spectral classification of Duc et al. (2002). A vertical solid line, and two dashed lines, identify the H α and [NII] lines, where H α is detected. Panel (a) shows the 13 sources detected only at $6.7\mu\text{m}$. Panel (b) shows the eight galaxies detected at $15\mu\text{m}$; all but two (ISO# 4, 28) are also detected at $6.7\mu\text{m}$. ISO#6 and #4 are associated with a structure behind the cluster at $z = 0.215$.

of H α luminosity, for all galaxies with H α fluxes above our detection limit. Note that the relative strength of [NII] and H α are not accurately measured for the broad-lined Seyfert ISO#41, as our method is appropriate only for narrow lines. Galaxies detected with *ISOCAM* are shown with error bars. Veilleux & Osterbrock (1987) have shown that galaxies in which $[\text{NII}]\lambda 6583/\text{H}\alpha > 0.55$ are almost always associated with non-thermal emission (i.e., Seyfert, LINERS and narrow line radio galaxies), rather than with HII regions (see also Kewley et al. 2001). Four of the MIR sources (including the $6.7\mu\text{m}$ source ISO#12) have ratios greater than this limit, although the 1σ error bars overlap this line. However, the H α fluxes are not corrected for stellar absorption, and thus the $[\text{NII}]\lambda 6583/\text{H}\alpha$ ratio is an overestimate. In particular, the galaxy numbers 31, 37 and 10 are known from their full optical spectra to have strong Balmer absorption lines (Duc et al. 2002). These three galaxies are all consistent with $[\text{NII}]\lambda 6583/\text{H}\alpha < 0.55$ if the absorption correction is at least 3\AA , which is not unreasonable. Therefore, the only galaxy for which we have unambiguous evidence for a non-thermal contribution to the H α emission is ISO#41, which was previously known to be a Seyfert I galaxy (Duc et al. 2002).

We also show in Figure 9 the H α -emitting cluster members within the *ISOCAM* field of view which are undetected in the MIR. All but one of these has $L_{\text{H}\alpha} < 10^{40} h^{-2} \text{ ergs s}^{-1}$, below the sensitivity of the *ISOCAM* survey, 0.15 mJy in the $6.7\mu\text{m}$ band. Thus, the *ISOCAM* survey is nearly complete in the detection of galaxies with H α emission greater than this luminosity limit, a result we discuss further in §4 (see Figure 11).

3.5 Post-starburst Galaxies

We finally consider the H α properties of those galaxies identified as k+a by Duc et al. (2002). These are galaxies with little or no [OII] emission, but strong Balmer absorption lines which indicate the presence of young stars. Such spectra have been interpreted as reflecting a post-starburst state (Couch & Sharples 1987; Poggianti et al. 1999; Balogh et al. 1999), or as dust-obscured starbursts (Poggianti & Wu 2000; Smail et al. 1999). We observed six galaxies classified in this way, and we show their continuum-subtracted spectra in the region of H α in Figure 10. Only one of these galaxies, the $6.7\mu\text{m}$ source ISO#12, was securely detected in H α . The H α luminosity of this galaxy is very low, at $0.3 \times 10^{40} h^{-2} \text{ ergs s}^{-1}$, corresponding to a star formation rate less than $0.1 h^{-2} M_{\odot} \text{ yr}^{-1}$. H α absorption is evident in all the remaining spectra except # 3828. In comparison, Balogh & Morris (2000) found that at least 2/6 of their k+a galaxies show H α emission. However, their definition of a k+a galaxy is stricter than that of Poggianti et al. (1999), which was adopted by Duc et al. (2002); furthermore, only ISO#12 is listed as a “confident” k+a galaxy by Duc et al. (2002), while the remainder are of uncertain classification. Hence, it is difficult to draw strong conclusions; but it is clear that there is little if any ongoing star formation in these galaxies, although they must have had at least some star formation in the recent past to give rise to the strong Balmer absorption.

4 DISCUSSION

Figure 2 demonstrates that, as was the case for the $z = 0.31$ cluster AC114 (Paper I), the number of H α emitters in A 1689 is well below that expected from the surrounding

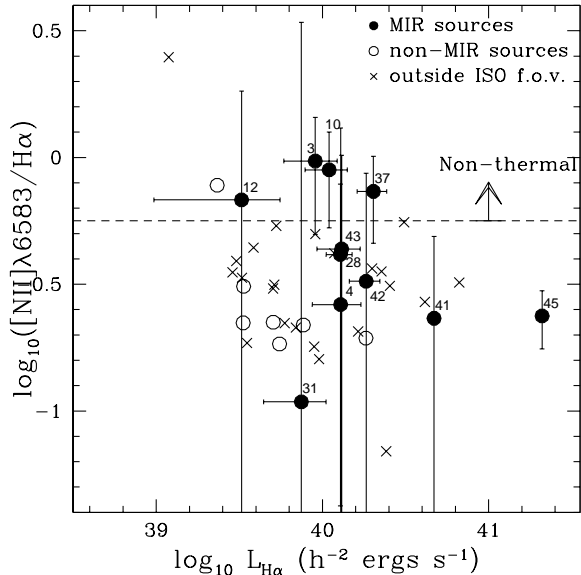


Figure 9. The ratio of $[\text{NII}]\lambda 6583/\text{H}\alpha$, for galaxies with $\text{H}\alpha$ and $[\text{NII}]$ flux above our detection limit. No absorption correction is applied, so these measurements overestimate the line ratio, particularly for the galaxies # 31, 37 and 10, which are known to have strong Balmer absorption. Galaxies detected with *ISOCAM* are shown as solid points with error bars; the *ISO* identification number from Fadda et al. (2000) is also shown. Open symbols are galaxies which lie within the *ISOCAM* field of view, but are not detected in the MIR. Crosses represent galaxies outside the *ISOCAM* field, so no MIR data is available. The horizontal, dashed line shows the flux ratio which divides non-thermal emission sources from line emission due to star formation, as labelled (Veilleux & Osterbrock 1987).

field, by about a factor ~ 5 . It is interesting to explore whether or not the difference between the cluster $\text{H}\alpha\text{LF}$ and that of the CFRS field can be entirely attributed to the difference in morphological composition. If we make the reasonable approximation that star formation is restricted to galaxies of type Sa or later (see §3.3), then we can renormalize the CFRS $\text{H}\alpha\text{LF}$ assuming that 65% of field galaxies at $z \sim 0.2$ are of this type (Abraham et al. 1996; Glazebrook et al. 1995). In §3.3 we determined that $\sim 20\%$ of the cluster members in our $\text{H}\alpha$ survey within the *HST* fields are of type Sa or later. Since the *HST* mosaic covers an area comparable to that of the LDSS++ field, we can appropriately renormalize the CFRS $\text{H}\alpha\text{LF}$, as shown as the short-dashed line in Figure 2. This renormalization reduces the discrepancy between the field $\text{H}\alpha\text{LF}$ and that of A 1689, but does not remove it; $\text{H}\alpha$ emitters are still $\gtrsim 50\%$ more abundant in the field. This discrepancy cannot be explained by assuming that star formation, in both the field and cluster, is mostly restricted to galaxies of type Sc or later. If this were the case, the CFRS $\text{H}\alpha\text{LF}$ of Figure 2 would be $\sim 50\%$ higher than assumed in Figure 2.

Thus, it appears that the lower star formation rate of the cluster galaxies is not due only to the difference in morphological composition, relative to the field. The next step is to look for evidence that $\text{H}\alpha$ emission in galaxies of a given morphological type is lower in clusters, relative to the field (e.g., Balogh et al. 1998). We will do this

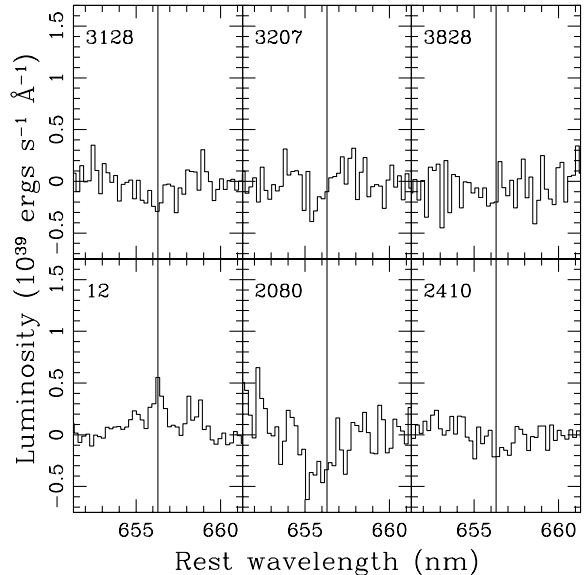


Figure 10. Continuum-subtracted, rest-frame LDSS++ spectra of galaxies classified k+a by Duc et al. (2002). Only galaxy 12 (a $6.7\mu\text{m}$ *ISO* source) is confidently classified k+a, and this is the only galaxy detected at $\text{H}\alpha$. The vertical, solid lines show the expected position of $\text{H}\alpha$ based on the redshifts of Duc et al. (2002).

by comparing our data with the local field galaxy sample of Jansen et al. (2000). Our sample is 50% complete to $I = 21$ (see Figure 1a), which corresponds approximately to $M_B = -15.9 + 5 \log h$, using the colour transformations in Fukugita et al. (1995). There are 173 galaxies in the sample of Jansen et al. (2000) brighter than this limit, and we take this as our comparison sample.

If we adopt the statistical background subtraction method and consider the results of the full sample (Figure 6b), the fraction of late-type galaxies in A 1689 detected in $\text{H}\alpha$ is $\gtrsim 90\%$ although this fraction is not very well determined, due to the small number of late-type galaxies and the uncertainty of the background correction. In the sample of Jansen et al. (2000), 104 of the 121 galaxies brighter than $M_B = -15.9 + 5 \log h$ classified as Sa or later show $\text{H}\alpha$ emission with $W_o(\text{H}\alpha) > 2\text{\AA}$. This fraction, 86%, is in excellent agreement with our results for A 1689. Thus, we do not find evidence that the few spiral galaxies in A 1689 are less likely to have $\text{H}\alpha$ emission, relative to their field counterparts.

Turning our attention to the early-type galaxy population, Jansen et al. find that 5/17 of their ellipticals and 7/25 of their S0 galaxies brighter than $M_B = -15.9 + 5 \log h$ show $W_o(\text{H}\alpha) > 2\text{\AA}$. Thus, 28% of their early-type galaxies show $\text{H}\alpha$ emission, compared with less than 10% in A 1689 cluster early-types (Figure 6). Even rejecting the three early-type galaxies in Jansen et al.'s sample with Seyfert nuclei, the fraction of early-type galaxies with $\text{H}\alpha$ emission is still twice as large as the fraction we find in A 1689.

These results suggest that the difference between the A 1689 $\text{H}\alpha\text{LF}$ and that of the CFRS, corrected to the same morphological composition, may be due to the fact that cluster E and S0 galaxies exhibit $\text{H}\alpha$ emission less frequently than their field counterparts. This cannot be tested directly,

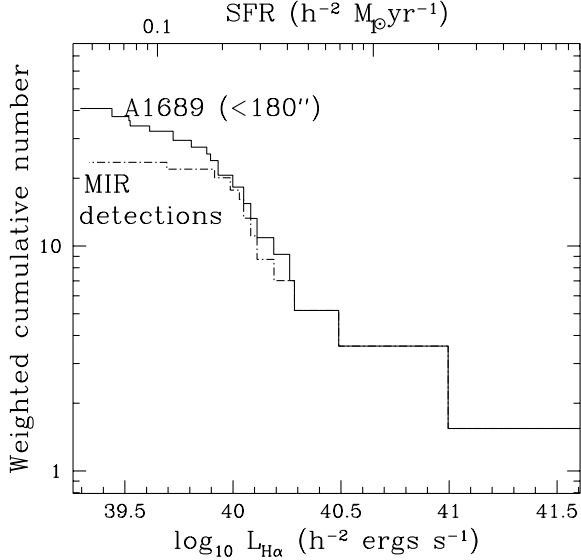


Figure 11. The $H\alpha$ luminosity function of A1689, restricted to the area covered by the ISOCAM survey of Fadda et al. (2000). We compare this with the $H\alpha$ luminosity function of those galaxies detected in the MIR.

as we do not have morphological classifications of the CFRS sample, and we depend upon the MDS sample of Abraham et al. (1996) being complete and representative, relative to the CFRS sample of TM98. However, we note that our results are in agreement with independent evidence from absorption line analysis that suggests that field early-type galaxies have younger stellar populations on average than their cluster counterparts (Abraham et al. 1999; Trager et al. 2000; Kuntschner et al. 2002). Our results could also be consistent with those of Balogh et al. (1998), who showed that disk-dominated galaxies in clusters have lower $[OII]$ emission than analogous galaxies in the field, if a substantial number of those disk-dominated galaxies are S0. On the other hand, Poggianti et al. (1999) found that the low star formation rates in clusters at $z \sim 0.4$ could be attributed to a large population of passive spiral galaxies. Our results do not appear to be consistent with such a population, although this is strongly dependent on the statistical subtraction of the field. Using only the spectroscopic sample of Duc et al. (2002) we find that only 60% of Sab galaxies are detected in $H\alpha$; it would be interesting to see if this holds for a larger sample of confirmed members.

We now consider the claims of Fadda et al. (2000) and Duc et al. (2002), that much of the star formation in A1689 is obscured by dust, and detectable in the MIR. We first reiterate that our observations are very sensitive to low $H\alpha$ fluxes, and we would detect a galaxy with a star formation rate greater than $\sim 3M_{\odot} \text{ yr}^{-1}$ unless it was obscured by more than 7 magnitudes of dust. We show the $H\alpha$ LF of our full sample, restricted to the $3'$ field of the ISOCAM survey of Fadda et al. (2000), in Figure 11. We compare this with the $H\alpha$ LF of galaxies detected in the MIR, within the same area. This demonstrates that the MIR catalogue is approximately complete to $H\alpha$ luminosities $L_{H\alpha} > 10^{40} h^{-2} \text{ ergs s}^{-1}$. However, our $H\alpha$ survey is at

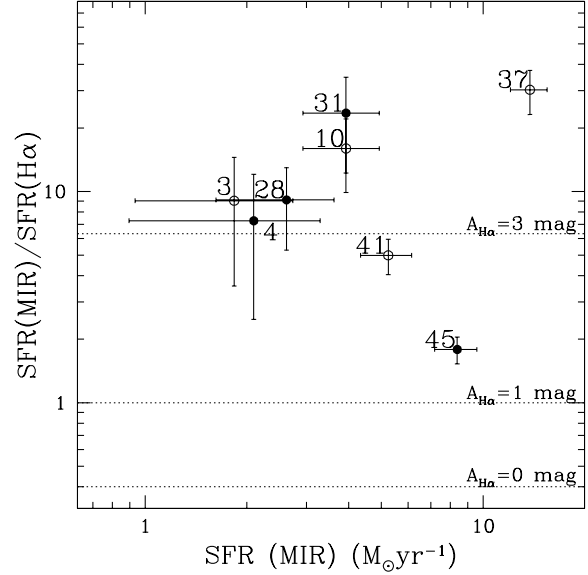


Figure 12. A comparison of star formation rates estimated from the $H\alpha$ emission line and those determined from $15\mu\text{m}$ fluxes (Duc et al. 2002). The $H\alpha$ -derived star formation rates assume an extinction of 1 magnitude. *Open symbols* are those galaxies with either broad $H\alpha$ emission, or $[NII]/H\alpha > 0.55$, possibly indicative of significant non-thermal contribution, in which case both star formation rates are overestimates. The ISO identification number is shown next to each point. The horizontal, *dotted lines* show the expected offset if the extinction is 0, 1 and 3 magnitudes at 6563\AA .

least four times more sensitive and detects twice as many star forming galaxies in this volume (which contribute an additional 16% to the total amount of star formation).

In Figure 12 we compare star formation rates measured from $H\alpha$ with those measured from $15\mu\text{m}$ luminosities, as estimated by Duc et al. (2002). We have increased the published MIR star formation rates by a factor of 1.3 to account for the different cosmologies assumed. For those MIR sources with a flux ratio $F_{15}/F_{K'} \leq 0.2$ we reduce the MIR-derived star formation rate by a factor of two, to correct for photospheric emission¹.

If the dust giving rise to the MIR emission is heated predominantly by star formation, then our direct comparison with the $H\alpha$ fluxes supports the conclusions of Duc et al. (2002) and Fadda et al. (2000), that optical line emission underestimates the star formation in $15\mu\text{m}$ sources. Star formation rates estimated from the $H\alpha$ line (which include a correction for 1 magnitude of dust extinction) are lower than those derived from the $15\mu\text{m}$ data by a factor of between 2 and 20 for most of the galaxies. If we were to correct the observed $H\alpha$ fluxes for an assumed 5\AA of stellar absorption, this would reduce the discrepancy to a factor of 1.7–10. The effect is more severe for star formation rates determined from

¹ Duc et al. actually recommend this correction be made for galaxies with $F_{15}/F_{K'} \leq 0.1$, but the only two other sources affected by our more generous limits are actually upper limits on the flux ratio.

the [OII] emission line, where the underestimate is a factor of 10 to 100 (Duc et al. 2002).

This suggests that some of the MIR-detected galaxies could be obscured by up to 3 magnitudes of extinction at 6563Å. The main remaining difficulty is to understand how much of the MIR emission in the *ISOCAM* sample arises from non-thermal activity. For galaxies of this luminosity, a 30% contribution to their bolometric infrared luminosity from AGN-heating is not unreasonable (Tran et al. 2001); in this case, the SFR estimated from both the MIR luminosity and the H α luminosity are overestimated. However, even if galaxies are bolometrically dominated by star formation, the bulk of their 15 μ m emission could still be coming from an AGN, especially in a MIR-selected sample (but see Spinoglio et al. 1995; Chary & Elbaz 2001). There are currently no published wide-field, local MIR surveys which can directly address this question, although such studies are underway (e.g., Aussel & Alexander 2001; La Franca et al. 2002). Preliminary results from the ELAIS survey suggests that only $\sim 30\%$ of 15 μ m sources are AGN-dominated, while 45% are starbursts and 15% are absorption line galaxies (La Franca et al. 2002). However, this mix is likely to be strongly redshift-dependent, and the AGN contribution at $z \sim 0.2$ depends on which of the AGN or starburst population is evolving more strongly with redshift (Roche & Eales 1999). For at least one of the eight 15 μ m-detected galaxies in our H α sample (ISO# 41) there is a clear contribution to the dust heating from an AGN source, and this could hold for up to half of the sample (including ISO# 3, 10, 37), depending on the uncertain correction for stellar absorption and the usefulness of the [NII] λ 6583/H α ratio as an indicator of non-thermal emission.

5 CONCLUSIONS

We have obtained LDSS++ spectroscopy for 522 galaxies over a field covering $\sim 1.1 \times 1.1 h^{-1}$ Mpc in the $z=0.18$ cluster A 1689. We find the following results:

- $24 \pm 4\%$ of cluster members more luminous than $M_R = -16.5 + 5 \log h$, statistically weighted to account for sampling-related selection effects, are confidently detected in H α emission above a flux limit of $4h^{-2} \times 10^{38}$ ergs s $^{-1}$, corresponding to a limiting star formation rate of $0.008 h^{-2} M_{\odot} \text{ yr}^{-1}$, assuming 1 magnitude of extinction.
- The normalization of the cluster H α luminosity function ($z = 0.18$) is a factor of ~ 5 lower than that of the field at $z \approx 0.2$, from TM98, and a factor of ~ 2 higher than that in our previous study of AC114 ($z = 0.31$).
- From the 199 galaxies for which we have *HST* *WFPC2* morphologies, as well as LDSS++ spectroscopy, we determine that $\sim 20\%$ of the cluster members (regardless of their H α properties) are of type Sa or later, much less than the $\sim 65\%$ expected in a sample of field galaxies. Like their field counterparts, these spiral galaxies have a high incidence of H α detection, $\gtrsim 90\%$. On the other hand, H α emission in early-type galaxies (E and S0) is less frequently observed than in similar galaxies in the field, based on the sample of Jansen et al. (2000).
- After renormalizing the CFRS H α LF (TM98) to account for the difference in morphological composition between the field and cluster samples a $\sim 50\%$ deficit of clus-

ter galaxies with H α emission remains. Combined with the high incidence of emission in cluster late-type galaxies, this suggests that the star formation rates of early-type cluster galaxies are suppressed, relative to their field counterparts.

- All of the galaxies detected in the 15 μ m mid-infrared band with *ISOCAM* are detected in H α . The MIR survey of Fadda et al. (2000) selects an approximately complete sample of H α -emitting galaxies with $L_{H\alpha} > 10^{40} h^{-2}$ ergs s $^{-1}$. Our deep H α survey probes ~ 4 times fainter than this, doubling the sample of detected star-forming galaxies and recovering an additional $\sim 16\%$ of all H α emission in the cluster.

- The population of H α -emitting galaxies in A 1689 appears to be associated with substructure in the immediate foreground and background of the cluster. The MIR detections trace the dynamics of the H α population, suggesting that they are related.

- Star formation rates derived from 15 μ m emission, neglecting a significant non-thermal component, are a factor 2–20 larger than those estimated from H α , assuming 1 magnitude of extinction. This difference is reduced to a factor $\lesssim 10$ if we account for an assumed 5Å underlying stellar absorption. Both star formation rate estimates may be overestimated if there is a significant contribution to the dust heating from AGN, for which there may be evidence in up to 50% of the eight 15 μ m sources we observe in H α .

In summary, the star forming galaxies in the core of A 1689 are significantly rarer than in the surrounding field. This may be due primarily to a suppression of star formation in S0 or elliptical galaxies. Our deep H α survey finds all 15 μ m MIR sources catalogued in this region, so there is no evidence for any star formation completely hidden at H α , although the estimated star formation rates from H α may be too low by assuming standard extinctions. This depends, however, on the largely unknown contribution of AGN-heated dust to the MIR flux.

ACKNOWLEDGEMENTS

We would like to thank P.-A. Duc, D. Fadda and B. Poggianti for providing their data prior to publication, and for making many useful suggestions regarding the comparison with the *ISOCAM* data. We also thank Jean-Paul Kneib for providing the NTT *I*-band image from which the sample was selected. Finally, we thank an anonymous referee for helpful criticisms. MLB is supported by a PPARC rolling grant for extragalactic astronomy and cosmology at the University of Durham. WJC acknowledges funding support from the Australian Research Council. IRS acknowledges support from a Royal Society URF and a Phillip Leverhulme Prize Fellowship. Based on observations made with the NASA/ESA Hubble Space Telescope, obtained from the data archive at the Space Telescope Institute. STScI is operated by the association of Universities for Research in Astronomy, Inc. under the NASA contract NAS 5-26555.

REFERENCES

- Abraham, R. G., Ellis, R. S., Fabian, A. C., Tanvir, N. R., & Glazebrook, K. 1999, MNRAS, 303, 641

- Abraham, R. G., van den Bergh, S., Glazebrook, K., Ellis, R. S., Santiago, B. X., Surma, P., & Griffiths, R. E. 1996, *ApJS*, 107, 1
- Alexander, D. M., Brandt, W. N., Hornschemeier, A. E., Garmire, G. P., Schneider, D. P., Bauer, F. E., & Griffiths, R. E. 2001, *AJ*, 122, 2156
- Almaini, O., Lawrence, A., & Boyle, B. J. 1999, *MNRAS*, 305, L59
- Aussel, H. & Alexander, D. M. 2001, American Astronomical Society Meeting, 198
- Balogh, M. L. & Morris, S. L. 2000, *MNRAS*, 318, 703
- Balogh, M. L., Morris, S. L., Yee, H. K. C., Carlberg, R. G., & Ellingson, E. 1997, *ApJL*, 488, 75
- . 1999, *ApJ*, 527, 54
- Balogh, M. L., Navarro, J. F., & Morris, S. L. 2000, *ApJ*, 540, 113
- Balogh, M. L., Schade, D., Morris, S. L., Yee, H. K. C., Carlberg, R. G., & Ellingson, E. 1998, *ApJL*, 504, 75
- Blain, A. W., Smail, I., Ivison, R. J., & Kneib, J.-P. 1999, *MNRAS*, 302, 632
- Bower, R. G. 1991, *MNRAS*, 248, 332
- Butcher, H. & Oemler, A. 1984, *ApJ*, 285, 426
- Charlot, S., Kauffmann, G., Longhetti, M., Tresse, L., White, S. D. M., Maddox, S. J., & Fall, S. M. 2002, *MNRAS*, 330, 876
- Chary, R. & Elbaz, D. 2001, *ApJ*, 556, 562
- Clowe, D. & Schneider, P. 2001, *A&A*, 379, 384
- Couch, W. J., Balogh, M. L., Bower, R. G., Smail, I., Glazebrook, K., & Taylor, M. 2001, *ApJ*, 549, 820
- Couch, W. J., Barger, A. J., Smail, I., Ellis, R. S., & Sharples, R. M. 1998, *ApJ*, 497, 188
- Couch, W. J. & Sharples, R. M. 1987, *MNRAS*, 229, 423
- Cowie, L. L., Songaila, A., & Barger, A. J. 1999, *AJ*, 118, 603
- Dressler, A., Oemler, A., Couch, W. J., Smail, I., Ellis, R. S., Barger, A., Butcher, H. R., Poggianti, B. M., & Sharples, R. M. 1997, *ApJ*, 490, 577
- Drinkwater, M. J., Phillips, S., Gregg, M. D., Parker, Q. A., Smith, R. M., Davies, J. I., Jones, J. B., & Sadler, E. M. 1999, *ApJL*, 511, L97
- Duc, P.-A., Poggianti, B. M., Fadda, D., Elbaz, D., Flores, H., Chaniel, P., Franceschini, A., Moorwood, A., & Cesarsky, C. 2002, *A&A*, 382, 60
- Durret, F., Gerbal, D., Lachieze-Rey, M., Lima-Neto, G., & Sadat, R. 1994, *A&A*, 287, 733
- Dwarakanath, K. S. & Owen, F. N. 1999, *AJ*, 118, 625
- Ellingson, E., Lin, H., Yee, H. K. C., & Carlberg, R. G. 2001, *ApJ*, 547, 609
- Fabian, A. C. & Iwasawa, K. 1999, *MNRAS*, 303, L34
- Fadda, D., Elbaz, D., Duc, P.-A., Flores, H., Franceschini, A., Cesarsky, C. J., & Moorwood, A. F. M. 2000, *A&A*, 361, 827
- Fadda, D., Flores, H., Hasinger, G., Franceschini, A., Altieri, B., Cesarsky, C. J., Elbaz, D., & Ferrando, P. 2002, *A&A*, 383, 838
- Flores, H., Hammer, F., Thuan, T. X., Cesarsky, C., Desert, F. X., Omont, A., Lilly, S. J., Eales, S., Crampton, D., & Le Fèvre, O. 1999, *ApJ*, 517, 148
- Fukugita, M., Shimasaku, K., & Ichikawa, T. 1995, *PASP*, 107, 945
- Genzel, R., Lutz, D., Sturm, E., Egami, E., Kunze, D., Moorwood, A. F. M., Rigopoulou, D., Spoon, H. W. W., Sternberg, A., Tacconi-Garman, L. E., Tacconi, L., & Thatte, N. 1998, *ApJ*, 498, 579
- Girardi, M., Fadda, D., Escalera, E., Giuricin, G., Mardirossian, F., & Mezzetti, M. 1997, *ApJ*, 490, 56
- Girardi, M., Giuricin, G., Mardirossian, F., Mezzetti, M., & Boschin, W. 1998, *ApJ*, 505, 74
- Glazebrook, K. & Bland-Hawthorn, J. 2001, *PASP*, 113, 197
- Glazebrook, K., Peacock, J. A., Miller, L., & Collins, C. A. 1995, *MNRAS*, 275, 169
- Iglesias-Páramo, J., Boselli, A., Cortese, L., Vílchez, J. M., & Gavazzi, G. 2002, *A&A*, 384, 383
- Jansen, R. A., Fabricant, D., Franx, M., & Caldwell, N. 2000, *ApJS*, 126, 331
- Kennicutt, R. C., J. 1998, *ARA&A*, 36, 189
- Kennicutt, R. C. 1992, *ApJ*, 388, 310
- Kewley, L. J., Dopita, M. A., Sutherland, R. S., Heisler, C. A., & Trevena, J. 2001, *ApJ*, 556, 121
- Kodama, T. & Bower, R. G. 2001, *MNRAS*, 321, 18
- Kuntschner, H., Smith, R. J., Colless, M., Davies, R. L., Kaldare, R., & Vazdekis, A. 2002, *MNRAS*, submitted
- La Franca, F., Matute, I., Fiore, F., Gruppioni, C., Pozzi, F., Vignali, C., & HELLAS, ELAIS collaborations. 2002, in *ASP Conference Series*, ed. R. Maiolino, A. Marconi, & N. Nagar, Vol. astro-ph/0109308
- Laurent, O., Mirabel, I. F., Charmandaris, V., Gallais, P., Madden, S. C., Sauvage, M., Vigroux, L., & Cesarsky, C. 2000, *A&A*, 359, 887
- Lilly, S. J., Tresse, L., Hammer, F., Crampton, D., & LeFèvre, O. 1995, *ApJ*, 455, 108
- Lutz, D., Spoon, H. W. W., Rigopoulou, D., Moorwood, A. F. M., & Genzel, R. 1998, *ApJL*, 505, L103
- Madau, P., Ferguson, H. C., Dickinson, M. E., Giavalisco, M., Steidel, C., & Fruchter, A. 1996, *MNRAS*, 283, 1388
- Margoniner, V. E., de Carvalho, R. R., Gal, R. R., & Djorgovski, S. G. 2001, *ApJL*, 548, L143
- Martin, C. L., Lotz, J., & Ferguson, H. C. 2000, *ApJ*, 543, 97
- Marzke, R. O., Geller, M. J., Huchra, J. P., & Corwin, H. G. 1994, *AJ*, 108, 437
- Metcalfe, N., Shanks, T., Campos, A., McCracken, H. J., & Fong, R. 2001, *MNRAS*, 323, 795
- Metcalfe, N., Shanks, T., Fong, R., & Jones, L. R. 1991, *MNRAS*, 249, 498
- Poggianti, B. M., Smail, I., Dressler, A., Couch, W. J., Barger, A. J., Butcher, H., Ellis, R. S., & Oemler, A. 1999, *ApJ*, 518, 576
- Poggianti, B. M. & Wu, H. 2000, *ApJ*, 529, 157
- Rigopoulou, D., Franceschini, A., Aussel, H., Genzel, R., van der Werf, P., Cesarsky, C. J., Dennefeld, M., Oliver, S., Rowan-Robinson, M., Mann, R. G., Perez-Fournon, I., & Rocca-Volmerange, B. 2000, *ApJL*, 537, L85
- Roche, N. & Eales, S. A. 1999, *MNRAS*, 307, 111
- Roussel, H., Sauvage, M., Vigroux, L., & Bosma, A. 2001, *A&A*, 372, 427
- Rowan-Robinson, M., Mann, R. G., Oliver, S. J., Efstathiou, A., Eaton, N., Goldschmidt, P., Mobasher, B., Serjeant, S. B. G., Sumner, T. J., Danese, L., Elbaz, D., Franceschini, A., Egami, E., Kontizas, M., Lawrence, A., McMahon, R., Norgaard-Nielsen, H. U., Perez-Fournon, I., & Gonzalez-Serrano, J. I. 1997, *MNRAS*, 289, 490
- Schechter, P. 1976, *ApJ*, 203, 297

Smail, I., Dressler, A., Couch, W. J., Ellis, R. S., Oemler, A., Butcher, H., & Sharples, R. M. 1997, *ApJS*, 110, 213
 Smail, I., Morrison, G., Gray, M. E., Owen, F. N., Ivison, R. J., Kneib, J.-P., & Ellis, R. S. 1999, *ApJ*, 525, 609
 Spinoglio, L., Malkan, M. A., Rush, B., Carrasco, L., & Recillas-Cruz, E. 1995, *ApJ*, 453, 616
 Struble, M. F. & Rood, H. J. 1999, *ApJS*, 125, 35
 Trager, S. C., Faber, S. M., Worthey, G., & González, J. J. . 2000, *AJ*, 120, 165
 Tran, Q. D., Lutz, D., Genzel, R., Rigopoulou, D., Spoon, H. W. W., Sturm, E., Gerin, M., Hines, D. C., Moorwood, A. F. M., Sanders, D. B., Scoville, N., Taniguchi, Y., & Ward, M. 2001, *ApJ*, 552, 527
 Tresse, L. & Maddox, S. J. 1998, *ApJ*, 495, 691
 Veilleux, S. & Osterbrock, D. E. 1987, *ApJS*, 63, 295
 Whitmore, B. C., Gilmore, D. M., & Jones, C. 1993, *ApJ*, 407, 489
 Wilman, R. J., Fabian, A. C., & Gandhi, P. 2000, *MNRAS*, 318, L11

APPENDIX A: A STATISTICAL, MORPHOLOGICALLY-DEPENDENT BACKGROUND CORRECTION

The redshifts of most galaxies in our sample which are not detected in $H\alpha$ are unknown; therefore a statistical correction needs to be applied to account for the fact that some of these will be field galaxies in the foreground and background of the cluster. In §2.1.4 we computed this correction for the global population by comparing the number counts in our field with those of Metcalfe et al. (1991). However, when we consider galaxies of a fixed morphological type, we need to consider the different morphological composition of the field. We take this from the *Medium Deep Survey* (MDS, Abraham et al. 1996; Glazebrook et al. 1995). The MDS comprises visual morphological classifications of a magnitude-limited field sample, from a survey of serendipitous *WFPC2* fields. These classifications are on the same scheme to that used here, as shown by comparisons in Smail et al. (1997). As in §3.3, we will consider four classes: Elliptical (E), S0 (including E/S0 and S0/a), Sab (including Sa, Sb, Sab) and Scd (including Sc, Sd, Scd and Irr). Over the magnitude range $I = 17$ –21, the field population is composed of 15% E, 20% S0, 30% Sab and 35% Scd, with only a small dependence on limiting magnitude. This is in reasonably good agreement with the distributions for the local field from Whitmore et al. (1993) (18% E, 23% S0 and 59% later types) and Marzke et al. (1994) (10% E, 30% S0, 40% Sab, 20% Scd at M^*).

Using the total field contamination estimate from Figure 1a, we can then determine the fraction of galaxies of each morphological type which are expected to be cluster members. From this number we subtract the fraction of galaxies of that type which we detect in $H\alpha$, yielding the fraction of undetected galaxies of that type which are expected cluster members. We show some sample numbers relevant to this calculation in Table A1. The first three columns show the galaxy type, the number and fraction of that type in the sample (ignoring the Uncertain class), and the number of galaxies detected in $H\alpha$. The rest of the calculation is best illustrated by a couple of examples. For this purpose, we

Table A1. STATISTICAL FIELD CORRECTIONS AT $I = 19$

(1) Type	(2) N_{gal}	(3) $N_{H\alpha}$	(4) f_{field}	(5) f_{cluster}	(6) $f_{\text{cluster}}^{\text{noH}\alpha}$
E	54 (27%)	2	6	78	74
S0	79 (40%)	4	8	80	75
Sab	28 (14%)	7	12	14	0
Scd	38 (19%)	10	12	37	11

will assume the field contributes 40% to the sample, which is the case at $I \sim 19$ (Figure 1a). Using the population mix presented above, we calculate that 6% of all galaxies in our sample are field ellipticals; this number is shown in column 4. We measure that 27% of our galaxies are ellipticals (column 2); therefore, we expect $(27 - 6)/27 = 78\%$ of these to be cluster members, and this number is shown in column 5. Only $2/54 = 4\%$ of these ellipticals are detected in $H\alpha$, so we expect $78 - 4 = 74\%$ of the undetected population to be cluster members. This final number is the one we are most interested in, and it is given in column 6. For the Scd class, this number is much smaller. We compare our measured fraction of 19% with the expected fraction of field Scd galaxies in our sample, 12% at $I \sim 19$, to determine that only 37% of Scd galaxies are cluster members. Since we detect $H\alpha$ in 26% of these galaxies, we conclude that only 11% of the undetected Scd galaxies are cluster members. In practice, these calculations account for the magnitude-dependence of the field contamination, and include the weights for the sampling fraction as a function of luminosity and radius (§2.1.4). Also, in some cases (see the Sab example in Table A1), the expected fraction of undetected cluster members is less than zero, reflecting the uncertainty and variation in the field composition. In this case, we assume that none of the undetected galaxies belong to the cluster.